Ultrafast probing of magnetic field growth inside a laser-driven solenoid

C. Goyon,[1] B. B. Pollock,[1] D. P. Turnbull,[1] A. Hazi,[1] L. Divol,[1] W. A. Farmer,[1] D. Haberberger,[2] J. Javedani,[1] A. J. Johnson,[1] A. Kemp,[1] M. C. Levy,[3] B. Grant Logan,[1] D. A. Mariscal,[1] O. L. Landen,[1] S. Patankar,[1] J. S. Ross,[1] A. M. Rubenchik,[1] G. F. Swadling,[1] G. J. Williams,[1] S. Fujioka,[4] K. F. F. Law,[4] and J. D. Moody[1]

[1]*Lawrence Livermore National Laboratory, Livermore, California 94551, USA*
[2]*Laboratory for Laser Energetics, University of Rochester, Rochester, New York 14623, USA*
[3]*Department of Physics, University of Oxford, Parks Road, Oxford OX1 3PU, United Kingdom*
[4]*Institute of Laser Engineering, Osaka University, Suita, Osaka 565-0871, Japan*

(Received 19 October 2016; published 31 March 2017)

We report on the detection of the time-dependent B-field amplitude and topology in a laser-driven solenoid. The B-field inferred from both proton deflectometry and Faraday rotation ramps up linearly in time reaching 210 ± 35 T at the end of a 0.75-ns laser drive with 1 TW at 351 nm. A lumped-element circuit model agrees well with the linear rise and suggests that the blow-off plasma screens the field between the plates leading to an increased plate capacitance that converts the laser-generated hot-electron current into a voltage source that drives current through the solenoid. ALE3D modeling shows that target disassembly and current diffusion may limit the B-field increase for longer laser drive. Scaling of these experimental results to a National Ignition Facility (NIF) hohlraum target size ($\sim 0.2\,\mathrm{cm}^3$) indicates that it is possible to achieve several tens of Tesla.

I. INTRODUCTION

Controlled magnetic fields applied to high-energy density (HED) plasmas is a promising area of research. Applied B-fields have been shown to increase electron and ion temperatures in laser-plasma experiments [1–3], which might help mitigate laser-plasma instabilities. Indirect drive ignition simulations show that a 20–60 T B-field applied to an imploding fuel capsule improves α particle and heat confinement relaxing the requirements for ignition [4]. In inertial confinement fusion experiments, higher neutron yields have been obtained with applied B-fields <10 T [5]. B-fields are also important for creating laboratory conditions scalable to astrophysical plasmas [6–11] and for creating and confining electron-positron pair plasmas [12].

Externally applied B-fields in HED experiments have achieved up to ~40 T [13] using pulsed power but are expensive to implement and not readily compatible with irradiation geometry and the cryogenic hardware required for ignition experiments [14]. Fundamental material properties prove to be a significant limitation to further increasing the field. However, an alternative laser-plasma-based technique has been shown to produce hundreds of Teslas. This technique, originally demonstrated by Korobkin [15], generated a B-field by focusing a laser onto a target made of two plates connected by a loop-shaped conducting strap. The mechanism that converts laser energy to B-field energy has been modeled as a laser-induced [21] or a hot-electron-generated [22,23] voltage between the plates, which drives current through the coil inductor. However, a comprehensive understanding of the physics underlying current generation in these laser-driven capacitor-coil targets remains elusive. Several groups have reported from hundreds of Teslas to multiple kiloTesla to be used on applications related to either astrophysical studies [11,16] or B-field assisted fast ignition [17–20]. None of the observations reported include a B-field measurement sampling directly the B-field in the center region of the coil. As a result, the amplitude of the central B-field requires

extrapolation from the actual measurement location using an unverified model for the spatial B-field topology. We believe this extrapolation is a primary contributor to the large variation in the reported B-fields values despite the use of similar laser drive and target geometry. In addition, there has been no detailed effort to describe the current dynamics inside of the coil during the laser drive.

In this article, we report on the simultaneous probing of the B-field at the center and the surrounding region of a laser-driven solenoid target using Faraday rotation and proton deflectometry as detailed in Sec. II. The data analysis used to reconstruct the B-field is described in Sec. III. The unique aspect of these results is that we have measured the temporal evolution of the B-field amplitude and topology: this provides the most accurate data available for testing models of the laser-generated B-field physics. In Sec. IV, we model the current flow inside the loop as a function of laser drive intensity using a lumped element circuit. We extrapolate these results showing that it is possible to achieve tens of Teslas inside a $0.2\,\mathrm{cm}^3$ NIF scale hohlraum using the laser-driven B-field generation scheme in Sec. V. Finally, we used ALE3D modeling of the coil to assess the current dynamics including Ohmic heating and coil explosion. Section VI details how the dynamic behavior of the laser driven coil could limit the achievable B-field on NIF.

II. EXPERIMENTAL DESCRIPTION

The experiments were conducted at the Omega-EP laser facility [24] using up to two long-pulse drive beams to generate the B-field and a short-pulse backlighter to generate the protons for deflection measurements. Figure 1 shows the experimental setup. The target is a 4-mm by 1.1-mm rectangle of 12.5-μm-thick gold foil that is molded into a U-shape. The separation between the two parallel plates is 0.5 mm and two 0.4-mm-diameter laser-entrance holes are cut near the bottom edge of the front side (side closest to the drive laser). The long-pulse
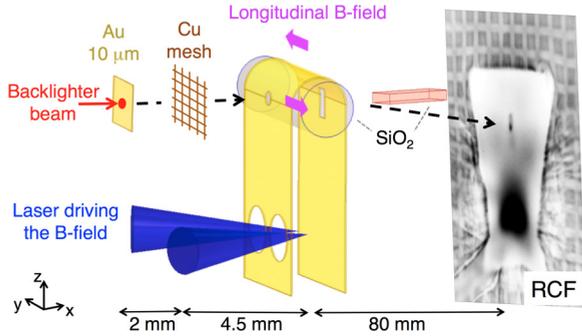
FIG. 1. Schematic of the experimental setup on Omega EP. TNSA protons generated at the gold foil drift perpendicular to the longitudinal B-field direction. A small sample of the protons passes through the coil by entering a 0.1-mm-diameter hole on the front plate and exiting a 0.1 * 0.25-mm slot on the rear plate. SiO_2 glass (inside and outside the coil) used for Faraday rotation is shown but is not present during proton measurements.

drive lasers with up to 1 TW at 351 nm in 0.75 ns (0.1-ns rise and fall with constant power for $\sim$0.55 ns) are directed through the holes in the front plate ($\sim$25° angle to the target normal) and focus to a 170-μm spot on the rear plate giving an intensity of $\sim$4.5 $\times$ 10^{15} W/cm^2. A 10-μm layer of CH is placed on the back plate to increase the density scale-length of the blow-off plasma and improve the efficiency of electron acceleration by nonlinear laser-plasma instabilities [25]. With the addition of the CH layer, we observed twice the B-field and a corresponding increase in the number and temperature of the hot electrons (approximately 30 to 60 keV) emitted from the rear plate. The laser-target interaction causes current to flow from the back plate through the coil and to the front plate, generating the solenoidal B-field directed from the left to the right inside the coil ($-\hat{y}$ direction), as shown in Fig. 1.

The Faraday rotation system [26] used a 10-ps, 10-mJ linearly polarized 263-nm probe beam directed along the axis of the solenoid, where it passed through two pieces of fused silica (SiO_2) glass. One piece was mounted inside the coil and the other outside to detect fringing fields. The B-field-induced polarization rotation of the probe is detected using Wollaston prisms to convert polarization rotation to brightness. X-ray-induced darkening [27] of the SiO_2 limits the Faraday measurements to $\leqslant$500 J of laser drive and probe timing of $<$1.5 ns. Two B-dot probes were used in some experiments but produced data that was not of sufficient quality to add to the understanding of the experiments.

A short-pulse laser generates protons for deflectometry measurements using the target normal sheath acceleration (TNSA) [28,29] technique. This laser focuses 200 J of 1053-nm light in 1 ps into a 10-μm spot on a 10-μm-thick gold foil positioned 6.5 mm away from the coil. The protons drift orthogonally to the solenoid axis where they are deflected by the **E** + **v** $\times$ **B** Lorentz force from the coil. Stray *E*-fields add uncertainty to the B-field estimate; we discuss their origin and effect below. The deflected protons are imaged onto a radiochromic film (RCF) pack composed of eight layers, sensitive to proton energy ranging from 3.6 to 30.2 MeV. A 65-μm period mesh grid, placed close to the Au foil, helps quantify the proton deflection. Most of the protons sample the
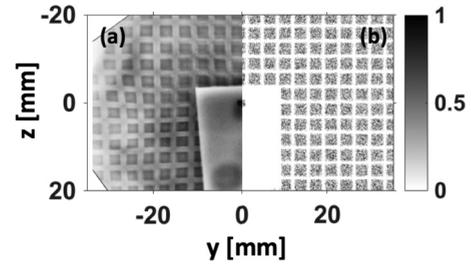

FIG. 2. (a) Normalized proton dose measured on the Radiochromic film sensitive to 29.5 $\pm$ 0.5 MeV protons without the drive beam. (b) Normalized synthetic RCF data without a magnetic field.

fringing field on the outside of the solenoid. However, a hole placed in the front plate and a vertical slot cut into the back plate allows a small sample of the protons to probe the main field at the center of the solenoid. These cutouts are shown in Fig. 1. Protons passing through the cutouts deflect down toward the laser-drive region; protons passing on the outside of the coil (through the fringing fields) deflect away from the coil.

III. B-FIELD TOPOLOGY RECONSTRUCTION

We restrict the analysis to proton energies greater than 29 MeV because this limits the temporal smear in the data to $<$50 ps. The analysis infers a B-field at the center of the coil through a two-step process. First, a current spatial distribution is prescribed in an ANSYS Maxwell [30] model of the coil to calculate the resulting three-dimensional B-field surrounding the loop. Second, a synthetic RCF image is constructed by simulating the trajectories of $>$10^6 protons from the source location to the RCF. The current amplitude is adjusted until the calculated proton image shows good agreement with the measurements.

The proton trajectory reconstruction is first validated by comparing simulations to a shot where no drive beams are used ("cold" radiograph). The experimental data [Fig. 2(a)] and the simulated image [Fig. 2(b)] are in good agreement. This step is critical to ensure the validity of the reconstruction method and will be used to assess the uncertainty in inferred fields.

Based on analytical calculations of transient fast-rising current flow inside a strap [31], we expect the current density spatial distribution to peak at the edges of the coil inside a few skin depths ($\delta \sim$2.5 μm for a 1 GHz current). Figure 3(a) is a simulated proton image for a uniform distribution of current across the conducting strap. This shows the greatest deflection of the coil silhouette at the coil center. Figure 3(c) is a simulated proton image with the majority of the current flowing in two equal regions at the coil edges. The edge current simulated image shows better agreement with the measurement in Fig. 3(b) in terms of the silhouette and grid deflection. All of the proton data consistently shows a target silhouette with greater deflection near the edges. Thus, an edge current distribution is used in all cases to infer the B-field amplitude. Sensitivity of the radiographs to current spatial distribution profile implies that the majority of the current flows in two $\leqslant$100-μm-wide regions at the coil edges.
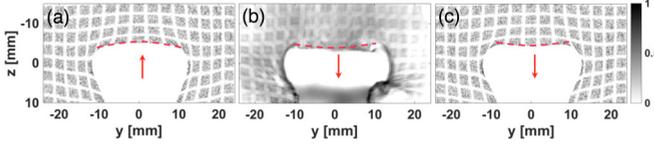
FIG. 3. (a) Synthetic RCF data for 180 kA of total current distributed uniformly across the length of the target. (b) Proton dose measured on the Radiochromic film sensitive to 29.5 ± 0.5 MeV protons 0.65 ns after the beginning of the drive beam. (c) Synthetic RCF data for 180 kA of total current distributed equally in two $\leqslant 100$-μm-wide regions at the edges of the solenoid. Red arrows and dotted lines indicate the curvature of the deflection at the top edge of the target

The B-field amplitude is estimated by comparing the synthetic and experimental data using up to three metrics: (1) the width of the coil silhouette, (2) deflection through the solenoid (central meas.), and (3) deflection in the fringing fields (external measurement). The resolution threshold on each metric is estimated to be ∼0.5 mm (or ∼10 T) based on measurements on the cold radiograph shown in Fig. 2. Figure 4(a) shows the proton data at $t = 0.32$ ns after the start of the laser drive; the numbered arrows label the three metrics. On all our shots, inferred B-fields from individual metrics agree within 20%, which we use to set an approximate error bar on the B-field amplitude. It confirms that the edge-peaked current distribution gives a B-field topology that matches the measurements throughout the laser drive and that the $\nabla n_e \times \nabla T_e$ [32] B-field inside the laser-produced plasma does not significantly contribute to the solenoidal B-field measurement. Figure 4(b) shows a 2D map of the longitudinal B-field amplitude, normalized to the longitudinal B-field at the center of the coil, in a plane centered between the plates ($x = 0$). The B-field topology is similar for all of the conditions investigated, therefore we will specify B to be the on-axis longitudinal value at the center of the coil for the remainder of the paper.

Figure 5(a) shows the central B-field as a function of time for a fixed drive intensity of 4.5×10^{15} W/cm². The B-field linearly increases from 16 T to reach 210 T at the end of the laser pulse. Figure 5(b) shows the inferred B-field at $t = 0.6 \pm 0.1$ ns after the beginning of the drive for three different laser intensities. Increasing the laser intensity from 1×10^{15} to 4.5×10^{15} W/cm² (at fixed spot size) produces an order of magnitude increase in the B-field. These data provide time and
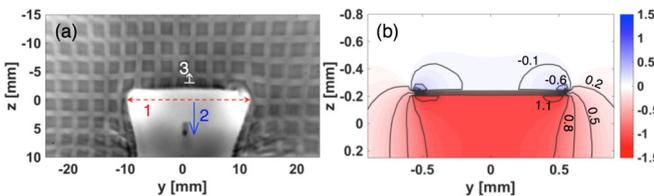

FIG. 4. (a) Normalized proton dose of the Radiochromic film sensitive to 29.5 ± 0.5 MeV showing the three metrics. Protons were delayed 0.32 ns after the beginning of the drive. (b) Contour plot of the longitudinal B-field (B_y) divided by the B-field value at the target center (corresponds to [y,z] = [0,0]).
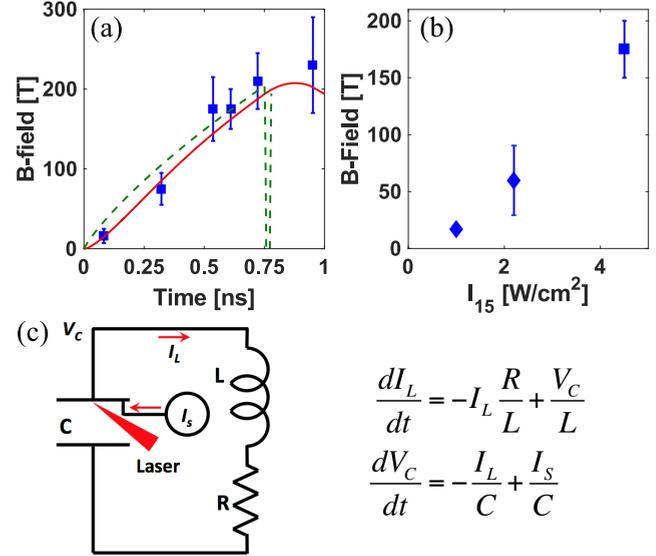

FIG. 5. (a) Squares correspond to experimentally inferred on-axis B-fields. Error bar shows the quadratic sum of each metric's uncertainty. The plain red (dashed green) line corresponds to the B-field amplitude obtained using the lumped-element circuit current for $C = 0.3$ nF (0.06 pF) (b) B-field at $t = 0.6 \pm 0.1$ ns after the beginning of the laser drive. Diamonds correspond to Faraday measurements and the square to proton deflectometry. (c) Lumped-element circuit of the laser-driven solenoid with coupled equations for the voltage between the plates, V_C, and the current inside the loop, I_L. I_S is the current source, C, L, and R are the target capacitance, inductance, and resistance.

intensity scaling of the B-field, which we can use to benchmark models for the laser coil system and extrapolate to a NIF hohlraum size laser driven coil.

IV. RLC MODELING

To describe the current and B-field time behavior we begin with a simple lumped-element circuit model sketched in Fig. 5(c). The equations describing the current and voltage behavior are written next to the circuit. The generation of the current can be described as follows: laser-generated hot-electrons leaving the rear capacitor plate collect on the front plate and induce a voltage difference between the two plates of the target. This capacitor voltage drives current through the inductor and regulates the continuing rate of charge buildup from the hot-electron current.

We numerically solved the circuit equation for I_L using the current source term $I_S = \frac{eh P_L}{2\kappa T_h}(1 + \frac{e V_C}{\kappa T_h})e^{-e V_C/\kappa T_h}$ [23] and $C = 0.06$ pF, $L = 0.4$ nH, $R = 0.02$ mΩ as estimated from the coil geometry used in the experiments. The conversion efficiency to hot-electrons h, varies from zero to 1 and $T_{hot} \sim 30$ keV. The resulting current through the loop I_L, is used as an input in Maxwell3D to obtain the B-field and allow direct comparison to the experiment. As a rule of thumb 1.2 kA equates to ∼1 T for the OMEGA EP target geometry. We are able to tune the model to reach 200 T at 0.75 ns by adjusting h to 0.1. However, the model, illustrated by the dashed line plotted in Fig. 5(a), shows two differences to the experimental
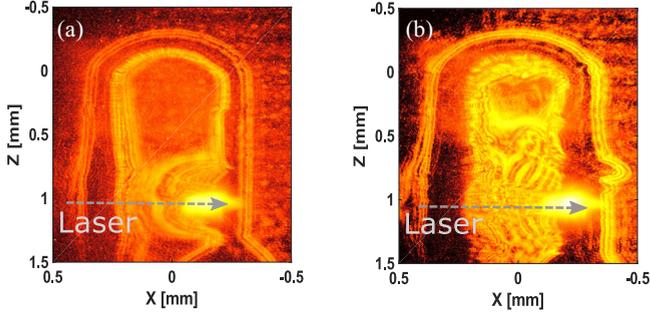
FIG. 6. (a) 4ω angular filter refractometer 250 ps after the beginning of the drive (b) 650 ps after the beginning of the drive. Laser is coming from the left hitting the rear plate (right plate) at $z \sim 1$ mm, the loop center is at $z = 0$ mm.

data: a more rapid initial increase of the field with time and high-frequency oscillations when the laser turns off (only one oscillation is shown). The more rapid initial increase of the field with time is attributed to the small value of C. The source current causes the voltage on the capacitor to spike very quickly (~ 25 ps) causing a rapid initial increase of the current through the loop. When the laser turns off, I_S drops to zero and the small capacitance induces high-frequency oscillations of the current with time period $\tau \sim 2\pi\sqrt{LC} = 31$ ps. A more linear increase in the B-field which matches the data better can be obtained by increasing C to 0.3 nF. This much larger C converts I_S to an approximately constant voltage source causing a quasilinear rise of B [solid line of Fig. 5(a)]. It is also consistent with the B-field continuing to increase after the laser turns off [at 0.95-ns delay on Fig. 5(a)] as the larger capacitance does not induce rapid oscillations once the laser shuts off. We note that using another expression for I_S [33] also requires an increased capacitance to match the data. The target capacitance is dictated by the plate geometry but also by the electric permittivity of the medium between the plates. Indeed, angular filter refractometer [34] measurements in Fig. 6 show a plasma plume expanding between the plates. Refraction contours of the probe due to the presence of plasma are observed near both plates at ~ 250 ps and plasma is filling the whole gap by 650 ps. Our hypothesis for increasing the target capacitance is that the plasma inside the gap shields the electric field between the plates [35] in several Debye lengths. This leads to a plate capacitance 3 to 4 orders of magnitude higher than the geometrical capacitance. A higher capacitance is plausible as soon as plasma expansion is enough to shield the electric field (tens of picoseconds). After the fast rise, the capacitance is expected to decrease with time because the temperature (Debye length) increases from laser heating. The lumped-element model provides good agreement with the results as long as $0.13 < C[\text{nF}] < 0.7$, which encompasses the expected time variation of the capacitance over the laser drive duration. A better characterization of the capacitance is beyond the scope of this paper. The need for a larger capacitor does not change if we include a small resistance in parallel with the capacitor to represent possible current flow through the plasma.

The model is further benchmarked against the experimental data using the intensity scaling shown in Fig. 5(b). We find, while keeping $T_{\text{hot}} = 30$ keV, that h must be increased from 0.001 to 0.015 when intensity increases from 10^{15} to 2.2×10^{15} W/cm^2. Doubling the laser intensity again gives $h \sim 0.1$, which is in good agreement with the conversion efficiency reported in Ref. [36] for a similar laser intensity. Above 5×10^{15} W/cm^2 experimental data from Ref. [36] suggest that the conversion efficiency saturates at ~ 0.1.

V. EXTRAPOLATION TO NIF

We can use our RLC model to estimate the expected field inside a NIF-size target without additional hypotheses by keeping the drive laser and the plate region similar to the Omega EP experiments. Increasing the coil size to ~ 5-mm diameter [37] increases the inductance to $L = 1.5$ nH [30] and should give a 9 T B-field. It is possible to further increase the B-field by overlapping four NIF quads thus increasing the drive intensity to 10^{17} W/cm^2. To estimate the B-field at higher intensity, we assume that h saturates at 0.1 and increase the hot electron temperature to 75 keV [38]. The current reaches 300 kA after 1 ns leading to a 30 T B-field at the coil center. This results suggests that the use of a laser driven coil is a promising method to achieve an external B-field over a large volume, ~ 0.2 cm^3 on NIF.

VI. DYNAMIC LIMITATIONS

The dynamics of the current flow through the coil is not described by the lumped-element circuit. The current rise to ~ 300 kA heats the coil edges causing the electrical resistance to increase rapidly and the edges to explode. This effect can be addressed using Arbitrary Lagrangian-Eulerian 3D Multi-Physics Code (ALE3D) [39]. A symmetric section of the target geometry is modeled using 650k mesh elements with a size of about 1 μm near the coil edges and increasing to 5 μm away from the edge. The results presented were unaffected by a smaller mesh size. The initial condition is no current, room temperature and the voltage from the lumped element circuit is a boundary condition. Calculations show a current density peaked at the coil edges in agreement with the experimentally inferred distribution. The coil resistance increases by a factor of a thousand, from ~ 0.02 to 20 mΩ during the laser drive due to coil heating; the coil inductance remains nearly constant at 0.4 nH. Increasing the resistance to 20 mΩ does not affect the B-field rise or maximum value estimated using the RLC model. In addition to the RLC parameters, the current distribution will also evolve as a function of time as ohmic heating causes the coil edges to explode. The beginning of the coil explosion can be seen on the right side of the target in Fig. 3(b). According to ALE3D, the heated material causes the current density to shift towards a cooler and less resistive part of the target (i.e., toward the center of the strap and from the inner to the outer surface of the conductor) ~ 300 ps after the beginning of the drive. This produces an "anomalous current diffusion," which is about 40 times faster than normal current diffusion ($\Delta x^2/\Delta t = \sigma \mu_0 = 75$ m^2/s, where σ is the material conductivity and μ_0 is the permeability of free space). Therefore, current dynamic diffusion will introduce a time-dependent topology of the B-field. According to our simulations, half of the current remains in two $\leqslant 100$-μm-wide

regions at the coil edges for the whole duration of the laser drive and confirms that our assumption on the current distribution is valid for drive shorter than 1 ns.

VII. CONCLUSION

In summary, proton deflectometry measurements on a "U-shaped" solenoid are used to infer an edge-peaked current distribution and a quasilinear B-field increase with time, reaching ∼210 T in 0.75 ns for a constant laser drive. The data also suggests that the B-field increases with drive intensity and longer drive duration. Based on these experimental data we developed a lumped element circuit model allowing us to estimate current for a different laser intensity. We show that models of current generation indicate a dynamic capacitance that is much larger than the geometrical capacitance and may result from the blow-off plasma. The lumped element circuit model shows that we can reach ∼30 T in a NIF-size laser-driven coil in 1 ns. Complementary ALE3D simulations show that the current dynamic diffusion and coil disassembly

due to ohmic heating will affect the B-field rise for longer drive durations. We note that utilizing a laser-driven B-field in HED experiments requires consideration of the extremely high loop voltage(∼MV/m) created inside the solenoid due to the rapid onset of the B-field. Voltage breakdown and plasma formation on the surface of the target preventing field penetration of the target geometry are important concerns. The ability to control the rate of onset of the field as well as a more complete understanding of the current generating mechanism will make it possible to mitigate these issues.

ACKNOWLEDGMENTS

[1] B. B. Pollock, D. H. Froula, P. F. Davis, J. S. Ross, S. Fulkerson, J. Bower, J. Satariano, D. Price, K. Krushelnick, and S. H. Glenzer, Rev. Sci. Instrum. **77**, 114703 (2006).

[2] D. H. Froula, J. S. Ross, B. B. Pollock, P. Davis, A. N. James, L. Divol, M. J. Edwards, A. A. Offenberger, D. Price, R. P. J. Town, G. R. Tynan, and S. H. Glenzer, Phys. Rev. Lett. **98**, 135001 (2007).

[3] D. S. Montgomery, B. J. Albright, D. H. Barnak, P. Y. Chang, J. R. Davies, G. Fiksel, D. H. Froula, J. L. Kline, M. J. MacDonald, A. B. Sefkow, L. Yin, and R. Betti, Phys. Plasmas **22**, 010703 (2015).

[4] L. J. Perkins, B. G. Logan, G. B. Zimmerman, and C. J. Werner, Phys. Plasmas **20**, 072708 (2013).

[5] M. Hohenberger, P.-Y. Chang, G. Fiksel, J. P. Knauer, R. Betti, F. J. Marshall, D. D. Meyerhofer, F. H. Seguin, and R. D. Petrasso, Phys. Plasmas **19**, 056306 (2012).

[6] M. Yamada, R. Kulsrud, and H. Ji, Rev. Mod. Phys. **82**, 603 (2010).

[7] J. F. Drake, M. Swisdak, H. Che, and M. A. Shay, Nature **443**, 553 (2006).

[8] W. Daughton, V. Roytershteyn, H. Karimabadi, L. Yin, B. J. Albright, B. Bergen, and K. J. Bowers, Nat. Phys. **7**, 539 (2011).

[9] G. Fiksel, W. Fox, A. Bhattacharjee, D. H. Barnak, P.-Y. Chang, K. Germaschewski, S. X. Hu, and P. M. Nilson, Phys. Rev. Lett. **113**, 105003 (2014).

[10] W. Fox, G. Fiksel, A. Bhattacharjee, P.-Y. Chang, K. Germaschewski, S. X. Hu, and P. M. Nilson, Phys. Rev. Lett. **111**, 225002 (2013).

[11] N. C. Woolsey, Y. A. Ali, R. G. Evans, R. A. D. Grundy, S. J. Pestehe, P. G. Carolan, N. J. Conway, R. O. Dendy, P. Helander, K. G. McClements, J. G. Kirk, P. A. Norreys, M. M. Notley, and S. J. Rose, Phys. Plasmas **8**, 2439 (2001).

[12] H. Chen, G. Fiksel, D. Barnak, P.-Y. Chang, R. F. Heeter, A. Link, and D. D. Meyerhofer, Phys. Plasmas **21**, 040703 (2014).

[13] B. Albertazzi, J. Béard, A. Ciardi, T. Vinci, J. Albrecht, J. Billette, T. Burris-Mog, S. N. Chen, D. Da Silva, S. Dittrich, T. Herrmannsdörfer, B. Hirardin, F. Kroll, M. Nakatsutsumi, S. Nitsche, C. Riconda, L. Romagnani, H.-P. Schlenvoigt, S. Simond, E. Veuillot, T. E. Cowan, O. Portugall, H. Pépin, and J. Fuchs, Rev. Sci. Instrum. **84**, 043505 (2013).

[14] O. V. Gotchev, J. P. Knauer, P. Y. Chang, N. W. Jang, M. J. Shoup, D. D. Meyerhofer, and R. Betti, Rev. Sci. Instrum. **80**, 043504 (2009).

[15] V. V. Korobkin and S. L. Motylev, Sov. Tech. Phys. Lett. **5**, 474 (1979).

[16] L. Gao, H. Ji, G. Fiksel, W. Fox, M. Evans, and N. Alfonso, Phys. Plasmas **23**, 043106 (2016).

[17] S. Fujioka, Z. Zhang, K. Ishihara, K. Shigemori, Y. Hironaka, T. Johzaki, A. Sunahara, N. Yamamoto, H. Nakashima, T. Watanabe, H. Shiraga, H. Nishimura, and H. Azechi, Sci. Rep. **3**, 1170 (2013).

[18] J. J. Santos, M. Bailly-Grandvaux, L. Giuffrida, P. Forestier-Colleoni, S. Fujioka, Z. Zhang, P. Korneev, R. Bouillaud, S. Dorard, D. Batani, M. Chevrot, J. E. Cross, R. Crowston, J.-L. Dubois, J. Gazave, G. Gregori, E. d'Humiéres, S. Hulin, K. Ishihara, S. Kojima, E. Loyez, J.-R. Marquès, A. Morace, P. Nicolaï, O. Peyrusse, A. Poyé, D. Raffestin, J. Ribolzi, M. Roth, G. Schaumann, F. Serres, V. T. Tikhonchuk, P. Vacar, and N. Woolsey, New J. Phys. **17**, 083051 (2015).

[19] G.-Q. Liao, Y.-T. Li, B.-J. Zhu, Y.-F. Li, F. Li, M.-C. Li, X. Wang, Z. Zhang, S.-K. He, W.-W. Wang, F. Lu, F.-Q. Zhang, L. Yang, K.-N. Zhou, N. Xie, W. Hong, Y.-Q. Gu, Z.-Q. Zhao, B.-H. Zhang, and J. Zhang, Matter and Radiation at Extremes **1**, 187 (2016).

[20] K. F. F. Law, M. Bailly-Grandvaux, A. Morace, S. Sakata, K. Matsuo, S. Kojima, S. Lee, X. Vaisseau, Y. Arikawa, A. Yogo, K. Kondo, Z. Zhang, C. Bellei, J. J. Santos, S. Fujioka, and H. Azechi, Appl. Phys. Lett. **108**, 091104 (2016).

[21] J. F. Seely, Appl. Phys. B **31**, 37 (1983).

[22] H. Daido, F. Miki, K. Mima, M. Fujita, K. Sawai, H. Fujita, Y. Kitagawa, S. Nakai, and C. Yamanaka, Phys. Rev. Lett. **56**, 846 (1986).

[23] C. Courtois, A. D. Ash, D. M. Chambers, R. A. D. Grundy, and N. C. Woolsey, J. Appl. Phys. **98**, 054913 (2005).

[24] J. Soures, R. McCrory, T. Boehly, R. Craxton, S. Jacobs, J. Kelly, T. Kessler, J. Knauer, R. Kremens, S. Kumpan, S. Letzring, W. Seka, R. Short, M. Skeldon, S. Skupsky, and C. Verdon, Laser Part. Beams **11**, 317 (1993).

[25] W. L. Kruer, *The Physics of Laser Plasma Interactions* (Addison-Wesley Publishing Co., Reading, MA, 1988).

[26] J. A. Stamper and B. H. Ripin, Phys. Rev. Lett. **34**, 138 (1975).

[27] R. A. London, D. H. Froula, C. M. Sorce, J. D. Moody, L. J. Suter, S. H. Glenzer, O. S. Jones, N. B. Meezan, and M. D. Rosen, Rev. Sci. Instrum. **79**, 10F549 (2008).

[28] S. C. Wilks, A. B. Langdon, T. E. Cowan, M. Roth, M. Singh, S. Hatchett, M. H. Key, D. Pennington, A. MacKinnon, and R. A. Snavely, Phys. Plasmas **8**, 542 (2001).

[29] S. P. Hatchett, C. G. Brown, T. E. Cowan, E. A. Henry, J. S. Johnson, M. H. Key, J. A. Koch, A. B. Langdon, B. F. Lasinski, R. W. Lee, A. J. Mackinnon, D. M. Pennington, M. D. Perry, T. W. Phillips, M. Roth, T. C. Sangster, M. S. Singh, R. A. Snavely, M. A. Stoyer, S. C. Wilks, and K. Yasuike, Phys. Plasmas **7**, 2076 (2000).

[30] http://www.ansys.com/Products/Electronics/ANSYS Maxwell.

[31] E. J. Tuohy, T. H. Lee, and H. P. Fullerton, IEEE Trans. Power Appar. Syst. **87**, 455 (1968).

[32] S. Eliezer, *The Interaction of High-Power Lasers With Plasmas* (IOP, Bristol, 2002).

[33] G. Fiksel, W. Fox, L. Gao, and H. Ji, Appl. Phys. Lett. **109**, 134103 (2016).

[34] D. Haberberger, S. Ivancic, S. X. Hu, R. Boni, M. Barczys, R. S. Craxton, and D. H. Froula, Phys. Plasmas **21**, 056304 (2014).

[35] F. C. Shure, J. Nucl. Energy, Part C **6**, 1 (1964).

[36] E. L. Dewald, O. L. Landen, L. J. Suter, J. Schein, J. Holder, K. Campbell, S. H. Glenzer, J. W. McDonald, C. Niemann, A. J. Mackinnon, M. S. Schneider, C. Haynam, D. Hinkel, and B. A. Hammel, Phys. Plasmas **13**, 056315 (2006).

[37] S. W. Haan, S. M. Pollaine, J. D. Lindl, L. J. Suter, R. L. Berger, L. V. Powers, W. E. Alley, P. A. Amendt, J. A. Futterman, W. K. Levedahl, M. D. Rosen, D. P. Rowley, R. A. Sacks, A. I. Shestakov, G. L. Strobel, M. Tabak, S. V. Weber, G. B. Zimmerman, W. J. Krauser, D. C. Wilson, S. V. Coggeshall, D. B. Harris, N. M. Hoffman, and B. H. Wilde, Phys. Plasmas **2**, 2480 (1995).

[38] F. N. Beg, A. R. Bell, A. E. Dangor, C. N. Danson, A. P. Fews, M. E. Glinsky, B. A. Hammel, P. Lee, P. A. Norreys, and M. Tatarakis, Phys. Plasmas **4**, 447 (1997).

[39] R. Rieben, D. White, B. Wallin, and J. Solberg, J. Comput. Phys. **226**, 534 (2007).